EUROPEAN FUSION DEVELOPMENT AGREEMENT

EFDA–JET–PR(02)11

C. P. Perez, H. R. Koslowski, G. T. A. Huysmans, P. Smeulders, T. C. Hender,
B.Alper, R. J. Hastie, L. Meneses, M. F. F. Nave, V. Parail, M. Zerbini
and JET-EFDA contributors

Type-I ELM Precursor Modes in JET

Type-I ELM Precursor Modes in JET

C. P. Perez[1], H. R. Koslowski[1], G. T. A. Huysmans[2], P. Smeulders[3], T. C. Hender[4], B. Alper[4], R. J. Hastie[4], L. Meneses[5], M. F. F. Nave[5], V. Parail[4], M. Zerbini[3] and JET-EFDA contributors*

[1]Institut für Plasmaphysik, Forschungszentrum Jülich, Trilateral Euregio Cluster, D-52425 Jülich, Germany
[2]Association Euratom-CEA, Cadarache, F-13108 St. Paul-lez-Durance, France
[3]Associazione Euratom-ENEA, Centro Ricerche Frascati, Italy
[4]Euratom/UKAEA Fusion Association, Culham Science Centre, Abingdon, UK
[5]Euratom/IST, Instituto Superior Tecnico, Lisbon, Portugal
** See annex of J. Pamela et al, "Overview of Recent JET Results and Future Perspectives", Fusion Energy 2000 (Proc. 18th Int. Conf. Sorrento, 2000), IAEA, Vienna (2001).*

Preprint of Paper to be submitted for publication in
Nuclear Fusion

Type-I ELM Precursor Modes in JET

C. P. Perez[1], H. R. Koslowski[1], G. T. A. Huysmans[2], P. Smeulders[3], T. C. Hender[4], B. Alper[4], R. J. Hastie[4], L. Meneses[5], M. F. F. Nave[5], V. Parail[4], M. Zerbini[3] and JET-EFDA contributors[6]

[1]Institut für Plasmaphysik, Forschungszentrum Jülich, Trilateral Euregio Cluster, D-52425 Jülich, Germany
[2]Association Euratom-CEA, Cadarache, F-13108 St. Paul-lez-Durance, France
[3]Associazione Euratom-ENEA, Centro Ricerche Frascati, Italy
[4]Euratom/UKAEA Fusion Association, Culham Science Centre, Abingdon, UK
[5]Euratom/IST, Instituto Superior Tecnico, Lisbon, Portugal
[6]See annex of J. Pamela et al, "Overview of JET Results", Fusion Energy 2002 (Proc. 19th Int. Conf. Lyon, 2002), IAEA, Vienna (2003).

Abstract. Clear low frequency (typically 5-25 kHz) coherent type-I ELM precursors have been identified in JET. They are detected through various diagnostics, especially in the ECE and Mirnov signals, but also on the SXR cameras and the multichannel O-mode edge reflectometer. The modes propagate in the direction of the ion-diamagnetic drift and are usually accompanied by a slight rise in the divertor D_α-emission. The precursors have a kink-like structure and are localized to a few cm inside the separatrix, in the pedestal region. The duration of the precursor before the ELM crash varies greatly: Usually, the precursors appear $\sim$0.2-1 ms before the ELM, but there are many cases where they become destabilized several tens of ms in advance of it. Longlived precursors are often seen to grow and shrink repeatedly and change their frequency and dominant n-numbers rapidly. The range of toroidal precursor mode numbers n which have been observed is 1-13, and parametric studies show that n seems to be mainly prescribed by a combination of the electron pedestal pressure and the (normalized) electron pedestal collisionality ν_e^*, with increasing ν_e^* leading to higher n-numbers. Above a certain edge collisionality (roughly $\nu_e^* \gtrsim$1-3) the precursors seem to be absent, indicating that a sufficiently high edge current is important to destabilize the precursors. The low-n precursors are known to be external kinks (also known on JET as Outer Modes), while experimental findings and their comparison with stability calculations suggest that the precursor modes with higher n are not pure external kinks but coupled ballooning-kink modes. Several hundred discharges have been analysed, and in discharges with low to moderate edge collisionality the precursors could be detected prior to most type-I ELMs, while prior to type-III ELMs the modes were not encountered. In spite of their regular occurrence, there is no evidence of the precursor mode growth rate rapidly accelerating before the ELM, indicating that type-I ELMs on JET are not triggered by these modes.

1. Introduction

Type-I ELMs [1–3] occur as quasiperiodic particle and heat losses near the plasma edge and are compatible with good confinement at high density. However, the energy losses associated with them are a concern for ITER due to the large transient heat loads expected on the divertor tiles [4, 5]. Although their existence has been known for many years, their physics is not well understood, and the search for ELM precursor activity which could shed light onto its origin and control possibilities has been performed in many devices.

In counter-injected discharges in ASDEX-Upgrade low frequency (20 kHz) coherent oscillations starting 1 ms before the ELM have been detected by ECE channels resonant approximately 2 cm inside the separatrix, and by coils picking up oscillations of B_r [6, 7]. Phase shift analysis using 3 toroidally distributed coils yielded $n = 5$-10 [7]. No similar precursor activity could be observed in co-injected discharges. In a further report, density profile oscillations with 17 kHz frequency in a counter-injected discharge were measured via reflectometry and associated with a type-I ELM precursor [8]. Later on, higher frequency (70-150 kHz) precursors were reported in co-injected NBI discharges [9], detected with a newly installed enhanced Mirnov diagnostic. Up to three modes are observed at a time, and the toroidal mode numbers range from $n = 3$ to 6.

Magnetic oscillations with 70-140 kHz prior to type-I ELMs have been observed in ohmic and ECRH-heated discharges in COMPASS-D [10, 11] and, in the example presented, start at least 0.4 ms before the ELM. They propagate in the direction of the electron diamagnetic drift and are often composed of two beating modes. From the ratio of the plasma rotation to the mode frequencies, toroidal mode numbers $n = 4$ and 5 were concluded.

On DIII-D a general broadband fluctuation level increasing 30-50 ms before type-I ELMs is seen, but no coherent magnetic precursors seem to be observed [12]. Occasionally, some burst-like density fluctuations are seen [13].

On JT-60U coherent density fluctuations near the plasma edge with 10-25 kHz frequency could be measured with reflectometry [14]. They are observed prior to most type-I ELMs and start approximately 200-500 μs before the ELM. The oscillations could not be detected on the magnetics.

In JET low frequency modes ($\sim$15 kHz) preceding giant ELMs[1] have been reported in [15]. They are observed within a few ms of the D_α-spike and have $n = 2$ and 4 in the example shown. Longer lived precursors at higher frequency ($f \sim 80$ kHz) and with high toroidal mode numbers (n = 3-12) are also observed [15, 16]. Although in [16] it is not explicitly stated whether the ELMs analysed are type-III or type-I/giant ones, this work is often cited in the context of type-III ELMs. However, Fig. 4 of [16] is devoted to a giant ELM, namely the same as Fig. 8 of [15].

In hot-ion H-Mode discharges [17] giant ELMs were generally preceded by so-called Outer Modes [18], although they have not been explicitly labeled as precursors. Having low mode numbers (n mostly 1 or 2) and frequency ($f \sim 5$-15 kHz), they could be very long-lived, occasionally existing up to hundreds of ms. Outer Modes have been identified as low-n external kinks [19].

Subsequent to the JET references cited above several improvements to diagnostics, data acquisition and MHD analysis codes were made. In this paper we will present and study in detail precursor activity found prior to type-I ELMs in general (not restricted to giant ones) on JET. The term “precursor” is used here in its more general definition to denote modes that systematically precede ELMs, while the term “trigger” is used to denote those modes whose growth rate rapidly accelerates prior to the ELM. ELM triggers are also ELM precursors, but ELM precursors do not have to be necessarily ELM triggers. The outline of this paper is as follows: Section 2. is devoted to the experimental observations for a class of lower frequency precursors observed, and the properties of lower and higher-n precursors will be compared in section 3..

[1] The term ’giant’ has not acquired a standardized meaning in the literature. Following [15] it is used at JET to denote bursts of D_α above a certain amplitude.

Section 4. gives an overview of the ideal MHD activity that, according to modelling calculations, can be expected at the plasma edge, and compares it to the experimental findings. Finally, a discussion of the results will be presented in section 5.

2. Experimental Observations

2.1. Magnetic Measurements

Compared to other MHD activity like internal kinks or NTMs, the precursors are much weaker and often hard to observe directly on the Mirnov signals. The duration of the precursor varies greatly: In most cases, the precursor appears ~ 0.2 to 1 ms before the ELM, but sometimes it becomes destabilised several tens of ms, or even longer, in advance of it. No evident reason or rule for the disparity of observed precursor lifetimes could be identified. As longlived precursors are easier to study with the diagnostics, use of them will often be made throughout the paper. In the time window of Fig. 1 three type-I ELMs and a sawtooth crash occur. The first ELM is preceded by a shorter precursor (~ 2 ms), shown in the zoom view, while the second and third ELMs have much longer ones (~ 30 ms), but are difficult to see here. Fig. 2 shows the corresponding spectrogram, where the precursors ($f \sim 18$ kHz) are marked by arrows. The first precursor can hardly be seen due to its short life. At their usual frequencies precursors shorter than 1 ms are difficult, or impossible, to discern on spectrograms due to the finite number of sampling points required for the Fourier analysis. A further problem is that the precursor's frequency is often comparable to that of many other MHD events (e.g. fishbones), and thus in discharges with lots of MHD activity the precursors might be difficult to see on the spectrograms.

The toroidal mode numbers can be inferred from mode number spectra as shown in Fig. 3, where the colours denote the toroidal mode numbers n. By making a Fourier decomposition of a toroidal set of Mirnov coils and analysing the phase shift of the fluctuations the n-numbers can be obtained. For the analysis a high resolution array of 5 coils, with toroidal angles $\Delta\phi$ gradually increasing from 1.7 to 15.9 degrees, was used, adequate for mode numbers $n \leq 11$. A subset of the coils with lower $\Delta\phi$ was employed if higher mode numbers needed to be resolved or simply to check the correctness of previous calculations. The coils are positioned close to the plasma boundary, with $r_{\text{coil}}/r_{\text{sep}}$ being roughly 1.2, depending on the plasma shape. It proves very useful for finding hidden activity to plot the mode numbers in a spectrogram-like way due to its twofold filtering: in frequency- and in phase-space. This increases the contrast and makes it possible to observe modes faintly visible on the spectrograms. To reduce the noise level of the plots, points are discarded when the amplitudes are below a user defined threshold or the fitting error of the mode number exceeds a certain amount. Positive and negative mode numbers are detected. Modes with negative n rotate in the opposite direction to modes with positive n. The convention used here is that modes with negative n rotate in the direction of the electron diamagnetic drift. For the 3 ELMs shown the precursors have $n = +8$. The range of toroidal precursor mode numbers which have been observed is 1-13. Precursors with $n > 11$ are seen rather seldom, and precursors with $n > 13$ seem not to occur at all. The upper limit of observed precursor n-numbers is most likely physically real and not imposed by a diagnostic limitation. Although the radial damping rate of magnetic perturbations increases with increasing mode numbers, even precursors with very high $n \sim$ 11-13 could still be clearly discerned above the noise level on Mirnov signals. Therefore, it should have been possible to detect eventually occuring precursors with slightly higher $n \gtrsim 13$ on the magnetics if they would have been present. As noted above, the toroidal spacing of the coils used is easily capable of resolving higher toroidal mode numbers, and for example other edge MHD activity with $n = 15$-20 has been detected.

In addition, one observes in Fig. 3 several broader bands of magnetic fluctuation with higher frequency ($f =$ 10-80 kHz) propagating in the direction of the electron diamagnetic drift (negative n), with n typically ranging from -1 to -8. These bands were already studied in [20] and named washboard modes. Washboard modes are plasma edge instabilities,

and neither their origin nor their driving force are known. Resistive ballooning modes have been discussed as a possible candidate to explain their origin in [20]. The physics of washboard modes is beyond the scope of this paper, but, without going into much detail, it is worth noting that washboard modes and ELM precursors interact, with the ELM precursors tending to inhibit the washboard modes. The physical mechanism behind this interaction could not be yet identified. For a detailed description of washboard mode dynamics and their consequences for the plasma edge the reader is referred to [21].

2.2. Mode Location and Structure

The precursors always occur near the separatrix, in the pedestal region. The radial location of the coherent precursors can be most easily seen on the ECE diagnostic. JET's ECE system consists of 48 heterodyne radiometers sampled with 250 kHz, measuring slightly below the plasma midplane. The spacing between resonant measurement radii is typically only 1 or 2 cm. Fig. 4 shows a set of edge ECE signals for our example, and Fig. 5 shows the respective ECE profile and the location of the separatrix, with an uncertainty of approximately 1 cm, as calculated by the EFIT equilibrium code. The channels at $a - 5.0$ cm and $a - 3.9$ cm measure near the top of the pedestal ($a =$ separatrix radius). The oscillations are most clearly seen 2.6 cm inside the separatrix, well inside the optically thick region, enhanced by the large temperature gradients in the pedestal. The temperature oscillations of the two longer precursors grow within 2 ms and then saturate in amplitude until 2 and 0.7 ms before the ELM, respectively, where they begin to grow again, albeit with growth rates that are much smaller than in the first growth phase. As in the case of the precursor prior to the first ELM the temperature oscillations grow only roughly linearly in time when approaching the crash. Concerning ECE channels further outward towards the separatrix one has to be cautious. When the density becomes too low, the plasma does not behave as a black body, and the radiation then detected at a given frequency can have contributions from different plasma regions (shine-through effect). The interpretation of the signal using a local model is then impossible. This shows up in the ECE profile, where the level of emission picked up rises again artificially (dotted part of the profile). Another complicating fact is that while it is difficult to locate the origin of the shine-through radiation picked up, the amount of shine-through itself is additionally modulated by the density oscillations caused locally by the mode, which reflectometry confirms to be present. The optical thickness τ has been evaluated in the cold plasma approximation (the formulas are given in [22], Tab. IV) for the channels resonant at $a - 2.6$ cm and $a - 1.4$ cm. The values obtained for τ strongly depend on the assumed shape of the edge density profile. At $a - 2.6$ cm $\tau =$ 4-11, while at $a - 1.4$ cm $\tau =$ 1.3-3.9. For optical thickness $\tau > 2$ is required. The marginal channel at $a - 1.4$ cm is thus dubious and should be disregarded. Hence, only ECE data from channels measuring at optically thick radii is taken into account.

Fig. 6 shows results from the coherence analysis of a Mirnov signals with the ECE channels. The colour in the first two plots depicts the value of the coherence and the phase of the cross spectral density, respectively, as a function of the frequency and distance to the separatrix. The coherence value increases towards the edge, and the phase shows no variations with radius, suggesting a kink-like mode, although this data could be produced as well by an island located between the last optically thick ECE channel and the separatrix. The values of the radial displacement shown in Fig. 6 are found to increase rather sharply at the edge, with displacements on the order of 1 cm. One can further see that for our $n = 8$ precursor the mode extent is not limited to $a - 2.6$ cm, where the oscillations were clearly visible in Fig. 4, but that large displacements also occur one channel further inwards, measuring at the pedestal shoulder, where the modest temperature gradient made them more difficult to observe directly on the ECE signal. The method used to obtain the displacement from the coherence analysis is described in appendix C of [20]. In general, the displacements observed typically range from 1 mm up to 1.5 cm.

The mode location is further verified by an edge reflectometer. JET's O-mode reflectometer system consists of 10 channels

with cut-off densities ranging from 6.0 down to $0.43 \cdot 10^{19}$ m^{-3}. In general the modes are seen on all channels or a subset of channels with lower cut-off densities, depending on the discharge density. The fact that the modes are seen on the channels with low cut-off densities, measuring at pedestal radii that normally include radii where the ECE suffers from shine-through, indicates that the precursors indeed extend from about the pedestal shoulder, as seen from ECE measurements, until at least fairly close to the separatrix. Fig. 7 shows the fringe-jump corrected traces for an $n = 8$ precursor together with the distance of their reflecting layers to the separatrix. Lacking a possibility to measure fast density profiles at the edge, the cut-off radii have been estimated by taking the line-averaged density of the edge interferometer cord to be the density at the top of the pedestal, and then linearly extrapolating to zero density at the separatrix. Allowing for a finite density in the SOL would move the radii of the channels with lowest cut-off density further outwards, possibly outside the separatrix. The oscillations show no phase inversions between channels, confirming that the mode has a kink-like structure, i.e. twisting parity, and is not a magnetic island.

With the inserted filters very little information could be obtained from the SXR cameras due to their low response at the plasma boundary and the line-averaging. Only strong enough precursors could be faintly detected through spectrograms of channels looking towards the plasma edge, consistent with a mode localised in the plasma periphery. For a camera viewing the plasma laterally from the low field side, comparison of channels looking towards the top and bottom of the plasma (tangentially towards the same flux surfaces) yielded no evident up-down amplitude asymmetry.

Finally, the precursor occurrence is normally accompanied by a slight increase of D_α-emission (Fig. 8). The increased D_α could arise from a small increase in particle and/or energy transport through the pedestal associated with the precursors.

2.3. Further Properties

The precursors are variable in the sense that they might grow and shrink repeatedly before the ELM or change their dominant n-numbers and frequency rapidly, at first sight without an apparent cause, that is, with no major changes in the main plasma parameters. Fig. 9 shows an example for the change in amplitude, where the n-spectrum and ECE signals show long intermittent $n = 7$ (orange) precursors at 10-15 kHz prior to two type-I ELMs at 21.1 s and 21.34 s. Between 21.0-21.1 s and 21.2-21.35 s the plasma current increased marginally from 2.49 to 2.53 MA, recovering the current lost by the preceding ELM, but whether this is really responsible for the mode behaviour in this particular case remains unclear. One can see that this is restricted to the plasma edge, the core MHD activity (e.g. a sawtooth precursor at 12 kHz and a 4/3 mode around 32 kHz) remains unperturbed. At ~ 45 kHz one can observe a further mode with similar frequency behaviour and higher $n \geq 10$ (for modes with higher mode numbers than given in the scale the colour of the mode saturates at the highest colour of the scale). A separate analysis with a reduced set of coils to resolve higher mode numbers yielded $n = 11$-13.

Fig. 10 shows an example in which the dominant precursor mode numbers change spontaneously within approximately 500 μs: starting with $n = 9$ (15 kHz), the dominant precursor becomes $n = 7$ (8 kHz) and finally $n = 5$ ($\sim$1 kHz). In spite of being observed at similar radii, the observed precursor frequencies are not proportional to their n-numbers. Considering the limited spatial resolution of the ECE measurements, the most likely explanation is that the various precursors differ slightly in their mode location and structure, and that this might indeed play a role in the final propagation frequency in a plasma region where changes in gradients and/or rotation velocities are expected to occur on a very short scale length.

Sometimes it happens that multiple precursors precede an ELM. An example is shown in Fig. 11 where a whole spectrum of modes could be detected. One can distinguish precursors with $n = 6$ ($\sim$ 9 kHz), a very long $n = 7$ ($\sim$ 13 kHz), an $n = 8$ ($\sim$ 18 kHz) and at sligthly higher frequencies further modes with $n = 9$ and 10. Around 50 kHz one sees a further very long lasting mode with unusually high mode number and frequency, for which a separate analysis with a reduced set of coils yielded $n = 11$-13. Further analysis revealed that the $n = 7$ mode dominates over a long time, but becomes

weaker shortly before the ELM. Simultaneously, the $n = 8$ mode becomes dominant until finally the ELM occurs. The other modes turn out to be much weaker.

In general, the observations described above suggest that there is a whole pool of mode numbers available for type-I ELM precursors, which can be explained by the closeness of rational surfaces due to the high shear near the separatrix. It seems that some minor local parameter modifications in the plasma periphery are sufficient to stabilise or destabilise individual modes and to change their frequency or the most unstable mode numbers.

It is difficult to say whether the precursors interact or not. Several cases like the one above have been observed where the weakening of one precursor was followed by the appearance or growth of another one, as if the modes were competing amongst themselves trying to inhibit each other. Alternatively, this could be again explained by spontaneous minor radial shifts of the mode rational surfaces, always possible as the current magnitude and distribution are not ideally constant, with respect to the radii with largest driving forces, namely pressure and/or current gradients. On the other hand, cases are also found where at least two precursors with comparable amplitude coexist with no signs of interaction. In any case the present data does not suggest ELMs originate from a nonlinear coupling or mutual reinforcement of these kind of precursors.

3. Comparison of low-n and high-n Modes

In the previous section it has been mentioned that the precursor mode numbers cover a wide range from n = 1-13. Precursors with low n = 1-3 were regularly observed in so-called hot-ion H-Mode discharges [17], and are seen in some conventional ELMy H-Mode discharges as well. Hot-ion H-Modes are characterised by very high ion temperatures achieved by applying NBI heating to a low density target. The low n modes occuring in them were not explicitly labeled as ELM precursors, and have been named Outer Modes (OMs) [18] due to their localisation at the plasma boundary. The situation is that not all OMs ended with an ELM, but ELMs were generally preceded by OMs. By analysing the phase and amplitude behaviour of the oscillations detected on multiple SXR channels and comparing them to modelling results, OMs have been identified as low-n external kinks [19]. Although there is a priori no sharp boundary in the transition from low to high n-numbers that would suggest the higher n precursors to be of a different nature; strictly speaking only the low n-modes are experimentally known to be external kinks. This makes a comparison of low-n with intermediate and higher-n precursors particularly interesting. It was not possible, however, to repeat the analysis of [19] for higher-n precursors. Many of the SXR diodes have suffered radiation damage in the D-T campaign, and the precursor oscillations in the remaining SXR channels were too faint (in contrast to the OM cases used by that time, which benefited from very high edge temperatures).

The characteristic rise in the level of D_α-emission has been often used in the past as a characteristic feature to identify the occurrence of OMs. This D_α-rise is qualitatively similar to that observed for higher-n precursors, already shown in Fig. 8.

As an example for low-n precursors, two giant ELMs with their respective OMs are depicted in Fig. 12, including a Mirnov signal and its respective spectrogram, as well as the spectrum of toroidal mode numbers. The precursors are composed of a dominant $n = 1$ component with up to ten or twelve harmonics, which is usually regarded as a sign of high (poloidal or toroidal) localisation. It has been observed that with increasing precursor n-numbers the number of harmonics decreases systematically. Hence, e.g. precursors with dominant $n = 2$ are usually composed of four or five harmonics, $n = 4$ precursors have mostly an $n = 8$ harmonic, and precursors with $n \geq 5$ usually do not show additional harmonics. Linked to this, the oscillations associated with lower-n precursors are, compared to higher-n precursors, much less sinusoidal.

Fig. 13 shows the radial displacement profile of an $n = 1$ precursor, together with the position of the pedestal shoulder,

obtained with the same procedure as for the $n = 8$precursor in Fig. 6. The remarkable difference compared to the $n = 8$ precursor is that the mode width of the $n = 1$ precursor does not extend as far as the pedestal shoulder or even further into the plasma but that the large displacements only occur within the pedestal radii, that is, further outwards. This could be due to the limited resolution of the ECE diagnostic, but this pattern occured systematically in several other cases, so it seems that low-n modes have a narrower extent with respect to the width of the transport barrier compared to higher-n modes.

Comparison of Mirnov signals of low and high field side coils initially suggested that precursors with low $n = 1$ or 2 show no strong inboard/outboard amplitude asymmetry, as is expected for external kinks, while with increasing n-numbers the ballooning character of the modes seemed to become gradually more and more accentuated. Figs. 14a,b compare the Fourier amplitudes of Mirnov signals of a low and high field side coil for a low and a high n precursor, respectively. For the main component of the $n = 1$ precursor the ratio of measured amplitudes is small, about 1.75, while for the $n = 8$ precursor it is very high, roughly 30, although the two coils on the low and high field side have a comparable distance to the separatrix (~ 22 cm in this discharge). But there is an effect that needs to be considered in interpreting the data and imposes an artificial inboard/outboard asymmetry of the signal amplitudes measured by coils even for modes that do not have ballooning character: In the cylindrical approximation the mode-induced magnetic fluctuations radially decay with $(r_{\text{mode}}/r_{\text{coil}})^m$, where m is the poloidal mode number of the mode. Within this approximation, the radial decay of the mode-induced fluctuations is therefore equally strong on the low and the high field side. If the mode itself does not have ballooning character, then coils on the low and high field side pick-up fluctuations of equal amplitude. In toroidal geometry, however, the poloidal structure of modes is distorted compared to the cylindrical case: the local poloidal wavenumber k_θ of the mode is higher on the high than on the low field side (e.g. tearing mode's o- and x-points are not distributed poloidally equidistant, but closer to each other on the high field side). The result is that the mode-induced magnetic fluctuations on the high field side are subject to a stronger radial decay due to the higher "local m" compared to the fluctuations on the low field side. The differing radial decay unavoidably introduces an artificial inboard/outboard asymmetry of the signal amplitudes measured outside the plasma by coils even if the mode itself does not have ballooning character. This effect becomes more pronounced with increasing poloidal mode numbers, and can become very large, making it difficult to check for the ballooning character of modes simply by comparing signals of low and high field side Mirnov coils. An estimate of this effect can be given by following a similar technique than used in [23]. One assumes a field aligned perturbation with $\vec{k} \cdot \vec{B} = 0$, and obtains for the ratio of poloidal wavenumbers of a mode the following expression

$$\frac{k_{\theta_2}}{k_{\theta_1}} = \frac{B_{\theta_1}}{B_{\theta_2}} \left(\frac{R_1}{R_2} \right)^2$$

Using EFIT a ratio of wavenumbers on the high/low field side of ~ 3.4 is estimated for the case of Fig. 14b, which, for high enough m, can indeed lead to signal amplitude asymmetries comparable to the ones measured. For low m-numbers the effect is not important because the ratio $(r_{\text{mode}}/r_{\text{coil}})$ is usually close to one in JET. This is further confirmed by the behaviour of the harmonics of the $n = 1$ precursor in Fig. 14a: Although the lower n components show nearly no difference in amplitude on the low and high field side, the difference in inboard/outboard amplitudes gradually increases with the harmonics' mode numbers, and becomes very pronounced for the higher harmonics.

In order to study the MHD mode propagation in the vacuum region and verify the above considerations, modelling calculations have been performed with the MISHKA code [24] using real JET geometry, with the discharge shape obtained from EFIT and taking the JET vessel to be ideally conducting, and taking into account the coordinates of the measuring coils. Low and high-n cases have been studied, and the distortion of the modes in the poloidal direction causes indeed a different radial behaviour on the low and high field side of the vacuum that agrees quantitatively very well with the

assumption made above. So, in contrast to what has been presumed in [25], and lacking a reliable estimate of the poloidal mode number m of the precursors, it has to be concluded that the magnetic data does not clarify whether the higher-n modes really have ballooning character or not, because the difference in inboard/outboard signal amplitudes could well originate from the effect described above. It has to be emphasized that the above effect is of general importance, and should be taken into account whenever magnetic fluctuations picked up on the low and high field side want to be compared.

Initial studies to determine parametric dependences of the precursor mode numbers on local quantities have been performed. The precursor mode numbers are mainly prescribed by edge densities and temperatures. Fig. 15a shows their distribution in n_e-T_e-space. The line-averaged electron density has been measured through interferometry using a vertical cord that views the plasma edge on the low field side, while the value for T_e is taken at the pedestal shoulder and measured via ECE. For the study of parametric scalings data from 52 discharges has been used . The discharges cover a wide range in parameter space, with $B = 2.4$-3.9 T, $I = 2.0$-4.0 MA, $q_{95} = 2.85$-4.6, $\delta = 0.22$-0.47, and $P_{\mathrm{NBI}} = 8$-17 MW (sometimes also combined with ICRH). Each point in the plots corresponds to an ELM precursor. If several precursors occured prior to an ELM, the dominant one has been selected, while in cases with a fast succession of precursors the first one has been taken (this convention has been chosen to exclude possible nonlinear effects arising from the preceding precursor). Alternatively, one may plot the mode numbers versus pedestal pressure and collisionality (Fig. 15b), where $\nu_e^* = 0.012 n_{e20} Z_{\mathrm{eff}} q_{95} R/(\epsilon^{3/2} T_{e\mathrm{keV}}^2)$, taking $Z_{\mathrm{eff}} = 1.5$. There is a gradual transition from low to high n-numbers with increasing pedestal collisionality . The pedestal collisionality determines the amount of bootstrap current for given pedestal gradients [26], with increasing collisionality leading to reduced bootstrap current. This data suggests the mode numbers to be determined by some interplay of the pressure gradient and the edge current driving force. One can see in Fig. 15b that keeping the pedestal pressure fixed and decreasing the collisionality (increasing edge current) leads to lower mode numbers, while increasing the edge pressure keeping the edge current fixed (which implies simultaneously raising the collisionality) raises the mode numbers. In both cases the transition from low to high n-numbers occurs in a relatively narrow region of parameter space. For low enough collisionality (high enough current) only low mode numbers were observed, independently of the pressure. On the other hand, in discharges with sufficiently high edge collisionality (roughly $\nu_e^* \gtrsim$1-3, depending on the discharge configuration) the precursors seem to be absent, indicating that a sufficiently high edge current is important to destabilize the precursors. The observed parameter dependence cannot be explained by considering only pure external kinks/peeling modes. Further types of instabilities need to be included. The pressure-current dependence indicated by the data might open the possibility to change the precursor mode numbers actively by in-shot current ramps. Furthermore, it is worth noting that the onset of OMs could be delayed through a slow current ramp down, thus decreasing the edge current, once the H-Mode phase was established [27].

It is worth comparing the experimentally observed parameter dependence with theoretical predictions. Some recent work using the ELITE code [28], in conjunction with the low n stability code GATO [29], has been performed to explore of the relationship between the calculated unstable toroidal mode number of edge instabilities and edge density, collisionality and bootstrap current [30–32], highlighting the importance of the edge current density for the edge MHD stability. In [30], inclusion of current in studies of the pedestal leads to a separate dependence of MHD stability on density and temperature, rather than just pressure, because of the strong collisional dependence of the bootstrap current. This is in agreement with the experimental results presented here. The stability calculations have shown that pedestal currents play a dual role in the MHD stability, stabilising high toroidal mode number ballooning modes through reduction of the edge magnetic shear, while at the same time providing drive for intermediate to low n peeling modes. The result is that coupled peeling-ballooning modes at intermediate n are often the limiting instability. Similar trends have been obtained in [31, 32]. In [31], a decrease in bootstrap current leads to an increase in the n-numbers of the unstable coupled peeling-ballooning

modes. In [32], a set of discharge equilibria with varying density is studied. At low density, the edge bootstrap current stabilises the higher n peeling-ballooning modes, which allows the lower n modes to dominate the instability. At high density, and collisionality, the higher n modes are no longer stabilised and become dominant before the lower n modes can grow. These trends are consistent with the experimentally observed parameter dependence presented here.
To date no evident dependence of the precursor mode numbers on the plasma triangularity could be identified. Further parametric studies are anticipated.

4. Modelling Results

To gain insight into the stability limits of the H-Mode pedestal region extensive numerical simulations have been performed. As starting point for the calculations the JETTO code is used [33], whose equilibrium module takes into account the H-Mode pedestal and calculates the edge magnetic surfaces self-consistently with the edge pressure gradient and edge current density including the bootstrap current contribution. The formulas employed to calculate the bootstrap current can be found in [26]. The H-Mode pedestal width is a free parameter chosen to match the experimental data, namely the pressure at the top of the pedestal. Ideal stability limits are then calculated with the HELENA [34] and MISHKA-1 [24] codes by multiplying the edge pressure gradient and the edge current independently with a constant, keeping the total current and energy content of the plasma fixed. Diamagnetic effects and resistivity were not taken into account for the calculations presented here. The higher order (cubic) finite elements used in all codes allow accurate equilibrium/stability calculations from $n = 0$ up to very high toroidal mode numbers ($n \leq 50$). For each equilibrium the stability of $n = 1$, 2, 3, 4, 6, 8, 10, 12,... modes have been calculated, using the JET vacuum vessel as an ideally conducting wall.
The instabilities found can be classified into three categories: ballooning modes (the most unstable ones having typically high $n > 10$), kink (peeling) modes (mostly low $n < 6$) and ballooning-kink modes (normally with medium n-numbers around 5 to 15). Due to their overlap, n-numbers on their own are in principle only of limited usefulness to classify the modes. The classification relies more on the driving forces and different mode structures as described below. Ballooning modes are driven by the pressure gradient, $\alpha = -\mu_0 p' q^2 / B_0^2 \epsilon$, and stabilised by shear, whereas kink (peeling) modes are driven by the edge current density and stabilised by pressure. Kink-ballooning modes are driven by both the pressure gradient and the edge current density.
Fig. 16 shows calculations for an ELMy H-Mode discharge, where the stability limits for the different mode types are displayed. The coloured areas show the stability limits of infinite-n ballooning modes as calculated by HELENA at different values of the normalised poloidal flux function near the edge ($\psi = 0.95$-0.99). In addition, the numbers displayed in the plot represent the n-numbers of the most unstable finite-n modes up to $n = 14$ at the respective α and edge current values as calculated by MISHKA. Without taking the finite-n modes into account, a second stable regime for ballooning-modes would exist at high edge currents. Normally kink-ballooning modes are the most unstable modes mainly in the proximity of both kink and ballooning stability limits.
As mentioned the mode structures of the three types of instability differ significantly. Fig. 17a shows plasma cross sections with the poloidal mode structures of an $n = 20$ ballooning, an $n = 12$ ballooning-kink and an $n = 3$ kink instability, respectively. The ballooning mode shows the expected large asymmetry of the mode amplitude on the high and low field side, and has a relatively broad radial extent. The $n = 3$ kink has a comparable inboard/outboard mode structure, a much narrower extent, particularly around the midplane, and shows, in contrast to the ballooning mode, large and broad mode displacements concentrated around the x-point. The ballooning-kink mode shows a mixture of these properties, with a much larger amplitude on the low than on the high field side, broad radial mode extent and distinct displacements around

the x-point.
Also in Fig. 17 the respective midplane radial displacement profiles are shown, and the vertical line around $\sqrt{\psi} = 0.97$ denotes the position of the pedestal shoulder, which is held invariant as the edge current and pressure are scanned. Thus, the extent of ballooning and ballooning-kink modes is comparable to the width of the transport barrier, while the $n = 3$ kink is narrower, consistent with the experimental results in section 3.. The kink-mode displacement increases sharply towards the separatrix, while the ballooning displacement peaks well inside it. Ballooning mode peak amplitudes occur at the position of maximum pressure gradient. Both ballooning and ballooning-kink modes are composed of several m-components, whereas the kink-mode shows only a small number of them.
As described in section 3., the experimental measurements confirm that lower-n precursors have a narrower radial extent compared to the higher-n precursors. This is consistent with the lower-n precursors being external kinks, and also suggests that the higher-n precursors are not pure external kinks but according to their mode width either peeling-ballooning or pure ballooning modes. In addition, the observed precursor n-numbers are mostly below $n = 10$, which according to modelling is rather too low for pure ideal ballooning modes. Hence, modelling results are consistent with the low-n precursors being ideal external kinks, while higher-n precursors are most likely to be ideal peeling-ballooning modes.

5. Summary and Discussion

The properties of a class of type-I ELM precursors that is commonly observed in JET ELMy-H discharges with coinjected NBI have been studied in considerable detail. Their characteristic features comprise: low frequency, mostly below 25 kHz, beginning typically 1 ms before the ELM crash, though sometimes much earlier, propagation in the direction of the ion diamagnetic drift, localisation in the pedestal region extending to the separatrix or beyond with no radial phase inversion, and a slight increase of the D_α-emission accompanying their occurrence. Radial mode displacements from 1 mm up to ~ 1.5 cm are observed.
Due to the closeness of rational surfaces near the separatrix combined with the short scale length on which quantities like pressure gradient, edge current density, plasma rotation or influence of neutrals change radially, one can expect each mode to have a narrow instability window that may be easily disturbed. The observations made of multiple precursors at similar radii, sometimes changing their toroidal mode numbers and frequency with no obvious reason, suggest that this is indeed the case.
A range of mode numbers $n =$ 1-13 has been observed, with the low-n precursors known to be ideal external kinks. A thorough comparison of low- and high-n precursors has been performed both in experiment and through modelling calculations and suggests the moderate-n precursors are peeling-ballooning modes (and not ballooning modes, which occur at higher n). Pure peeling modes are precluded by the observation of the mode width, which is too broad for peeling modes, and because of the observed dependence of mode number on n_e and T_e (cf. Fig. 15). It rather seems that the precursor n-numbers are determined by some interplay of both the pressure gradient and the edge current density. Due to the absence of radial phase inversions magnetic island modes should be excluded.
If the precursors are involved at all in the ELM cycle, they seem not to be the actual trigger for the ELM. This is concluded from the observation that the precursor oscillations do not grow exponentially into the ELM crash but mostly rather linearly. In fact, there is no evidence of the precursor mode growth rate rapidly accelerating before the ELM, and cases were shown where the precursor amplitude even remains saturated over longer times until the ELM occured. A further point that suggests that the ELM precursors do not trigger the ELMs has been previously given in [27]: The technique of current rampdown used to optimise the performance of hot-ion H-Mode discharges was found to delay the onset of the low-n precursors (OMs) while making the ELMs appear earlier (ELMs were still preceded by the OMs in the current rampdown

discharges, but the duration and severity of the OMs was reduced compared to the discharges without current rampdown). This implies that the ELM trigger behaved differently to the OMs during the current rampdown, indicating that ELM precursor and ELM trigger are two separate phenomena. This and the large variation in the time by which the precursor appearance precedes the ELM could be explained in terms of the ELM event resulting from a combination of two instabilities. Within this picture a precursor mode starts once the stability limit for the first instability is encountered, but the ELM is not triggered until the stability limit for the second instability is reached. The model of the peeling-ballooning-cycle for type-I ELMs [35] points very much in that direction. However, if one assumes ELMs to be finally triggered by a combination of kink- and ideal ballooning-modes, at least in the particular case of discharges with low-n precursors, the kink-limit is obviously reached *before* the ideal ballooning limit, which is in conflict with the order of events predicted in the peeling-ballooning cycle originally proposed in [35]. A generalisation of the peeling-ballooning model with ELM cycles for which the kink/peeling boundary is encountered first has been recently proposed in [30].

On the other hand, the precursors seem to be absent in discharges with sufficiently high electron edge collisionality (strong gas puffed discharges) for which ν_e^* is roughly above 1-3 (depending on the discharge configuration), and also optimised shear discharges were reported where they could not be seen [36], raising the question whether the precursors are really linked to the ELM event. The absence of precursors in high collisionality discharges is not believed to be related to a diagnostic limitation. Although in many of these cases the ECE data are not available (making it difficult to find shortlived precursors, in particular), sufficiently longlived precursors should be still detectable through the magnetics. However, they have not been detected in spite of the considerable number of high density discharges analysed. This is in contrast to what is observed in discharges with low to moderate collisionality. Gas scans of discharges have been analysed in which the precursors still had relatively low $n = 5$-6 for a number of discharges at moderate fuelling rates, prior to their disappearance at the next highest density. The lack of precursors at high collisionality (low edge current) would be again consistent with their identity as ideal kink- or coupled ballooning-kink modes, and not ideal ballooning modes. A hypothesis that is supported by the overall data presented here is that the ideal ballooning modes, and not ideal kink- or coupled ballooning-kink modes, could provide the trigger for type-I ELMs. In this respect, certain theoretical works [37, 38] predict a general explosive feature of the ideal ballooning instability ("detonation") emerging from non-linear effects through the development of fine-scale substructures ("fingers"). In any case, the importance of the ELM precursors studied here relies in that they provide a valuable source of information to improve the understanding of ELM-cycles, and their further study certainly opens the possibility to validate, or refute, present ELM models.

The precursor phenomenon seems not to be restricted to JET. The precursors show similarities with the ones reported in [6–8, 14], particularly their low frequency and typical duration of about 1 ms, as well as the mode numbers reported in [6, 7].

A significant feature of ELMy H-Modes in JET is the universally observed washboard modes [20]. The properties of these modes, which seem to significantly interact with the ELM precursors, will be discussed in a future paper [21].

Acknowledgements

This work has been performed under the European Fusion Development Agreement.

References

[1] Zohm, H., Plasma Phys. Control. Fusion **38** (1996) 105.

[2] Connor, J.W., Plasma Phys. Control. Fusion **40** (1998) 191.

[3] Connor, J.W., Plasma Phys. Control. Fusion **40** (1998) 531.

[4] Leonard, A. W., et al, J. Nucl. Mater. **266-269** (1999) 109.
[5] Janeschitz, G., J. Nucl. Mater. **290-293** (2001) 1.
[6] Suttrop, W., et al, Plasma Phys. Control. Fusion **38** (1996) 1407.
[7] Kass, T., et al, Proc. 24th EPS Conf. on Controlled Fusion and Plasma Physics (Berchtesgaden), vol. 21A, ed M. Schittenhelm et al (Geneva: EPS) part IV, p. 1521 (1997).
[8] Manso, M., et al, Plasma Phys. Control. Fusion **40** (1998) 747.
[9] Maraschek, M., et al, Proc. 25th EPS Conf. on Controlled Fusion and Plasma Physics (Praha), vol. 22C (1998), 492.
[10] Buttery, R. J., et al, Proc. 21th EPS Conf. on Controlled Fusion and Plasma Physics (Bournemouth), vol. 19C, part III, p. 273 (1995).
[11] Colton, A. L., et al, Plasma Phys. Control. Fusion **38** (1996) 1359.
[12] Zohm, H., et al, Nucl. Fusion **35** (1995) 543.
[13] Doyle, E. J., et al, Phys. Fluids B **3** (1991) 2300.
[14] Oyama, N., et al, Plasma Phys. Control. Fusion **43** (2001), 717.
[15] Nave, M. F. F., et al, JET Report JET-P(95)03.
Nave, M. F. F., et al, International Conference on Plasma Physics ICPP 1994 (Foz do Iguacu, Brazil 1994) AIP Conference Proceedinds 345, American Institute of Physics 1995, p. 58.
[16] Ali-Arshad, S., et al, Proc. 19th EPS Conf. on Controlled Fusion and Plasma Physics (Innsbruck), vol 16C, part I, p. 227 (1992).
[17] JET Team (presented by Jones, T.T.C.), Plasma Phys. Control. Fusion **37** (1995) A359.
[18] Nave, M. F. F., et al, Nucl. Fusion **37** (1997) 809.
[19] Huysmans, G. T. A., Hender, T. and Alper, B., Nucl. Fusion **38** (1998) 179.
[20] Smeulders, P., et al, Plasma Phys. Control. Fusion **41** (1999) 1303.
[21] Perez, C. P., et al, 'Washboard Modes as ELM-related events in JET', submitted to Plasma Phys. Control. Fusion
[22] Bornatici, M., Cano, R., de Barbieri, O. and Engelmann, F., Nucl. Fusion **23** (1983) 1153.
[23] Snipes, J. A., et al, Proc. 29th EPS Conf. on Controlled Fusion and Plasma Physics (Montreux), P1.057 (2002).
[24] Mikhailovskii, A. B., et al, Plasma Phys. Rep. **23** (1997) 844.
[25] Perez, C. P., et al, Proc. 29th EPS Conf. on Controlled Fusion and Plasma Physics (Montreux), P1.023 (2002).
[26] Sauter, O. and Angioni, C., Phys. Plasmas **6** (1999) 2834.
[27] Nave, M. F. F., et al, Nucl. Fusion **39** (1999) 1567.
[28] Wilson, H. R., Snyder, P. B., Huysmans, G. T. A., and Miller, R. L., Phys. Plasmas **9** (2002) 1277.
[29] Bernard, L. C., Helton F. J. and Moore, R. W., Comput. Phys. Commun. **24** (1981) 377.
[30] Snyder, P. B., et al, Phys. Plasmas **9** (2002) 2037.
[31] Mossessian, D. A., et al, Plasma Phys. Control. Fusion **44** (2002) 423.
[32] Leonard, A. W., et al, Phys. Plasmas **10** (2003) 1765.
[33] Cenacchi, G., Taroni, A., Rapporto ENEA RT/T1B 88 (5) 1988.
[34] Huysmans, G. T. A., et al, Proc. CP90 Conf. on Comp. Physics, ed. A. Tanner (World Scientific Singapore 1991), p. 371.
[35] Connor, J. W., Hastie, R. J., Wilson, H. R., Phys. Plasmas **5** (1998) 2687.
[36] Alper, B., et al, Proc. 29th EPS Conf. on Controlled Fusion and Plasma Physics (Montreux), P1.025 (2002).
[37] Hurricane O A, Fong B H, Cowley S C 1997 *Phys. Plasmas* **4** 3565
[38] Fong B H 1999 *PhD thesis*, available at http://www.asp.ucar.edu/∼bhlfong/thesis.pdf

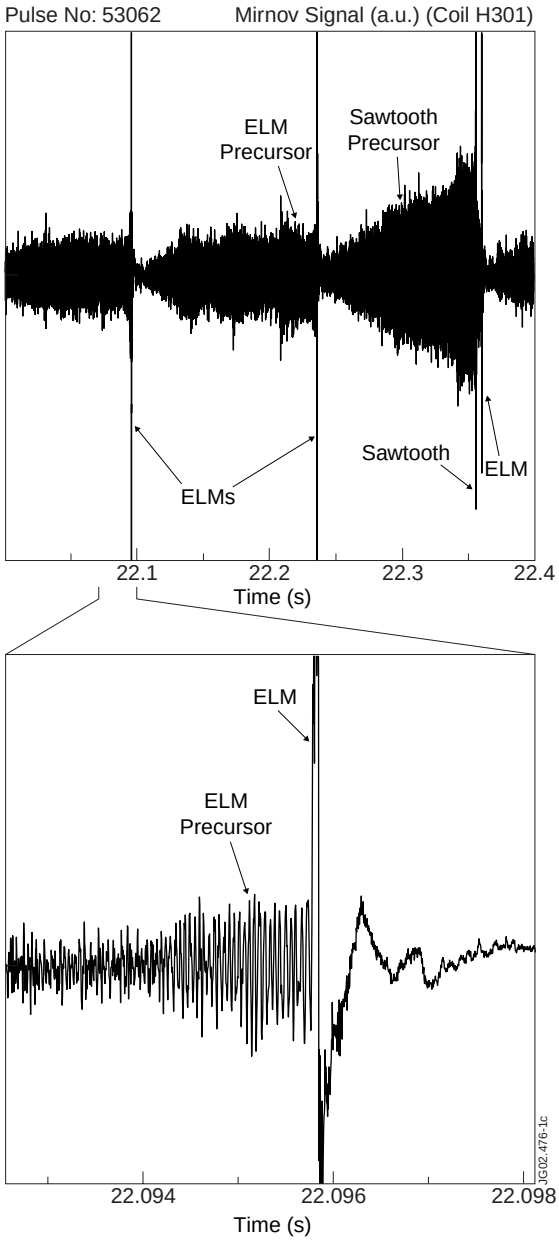

Figure 1: Mirnov signals of a coil located at the low field side for Pulse No: 53062. The parameters of this discharge at the relevant time were:
$B = 2.7T, I = 2.5MA, P_{NBI} = 13.2MW$ (co-injected), $\bar{n}_e = 7 \times 10^{19}\ m^{-3}$, $\kappa = 1.75$, $\delta_{u/l} = 0.36/0.24$

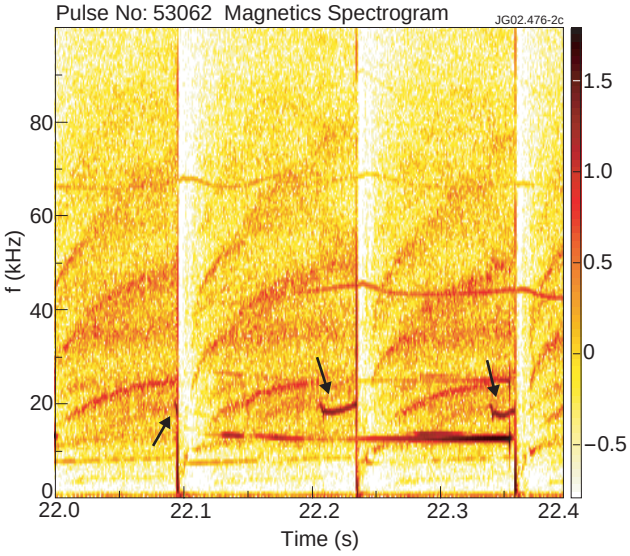

Figure 2: Magnetics spectrogram from a coil located on the low field side, with the precursors being marked by the arrows. The stronger mode at 13kHz is the sawtooth precursor. The colour scale for the amplitudes is logarithmic (log10).

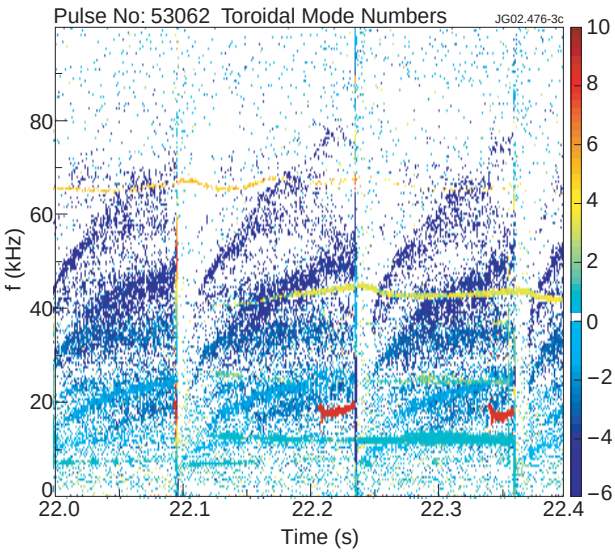

Figure 3: Spectrum of toroidal mode numbers n. The ELM precursors have n = 8 (red).

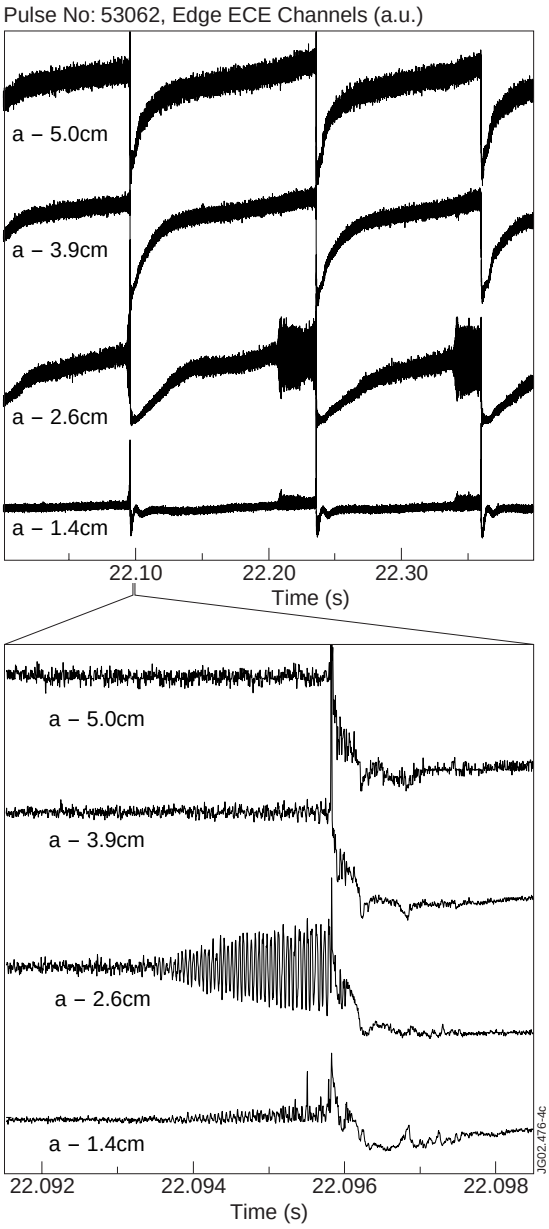

Figure 4: Edge ECE signals together with the distance of the measurement radii to the separatrix as calculated by EFIT. The second picture shows a zoom of the shorter precursor prior to the first ELM.

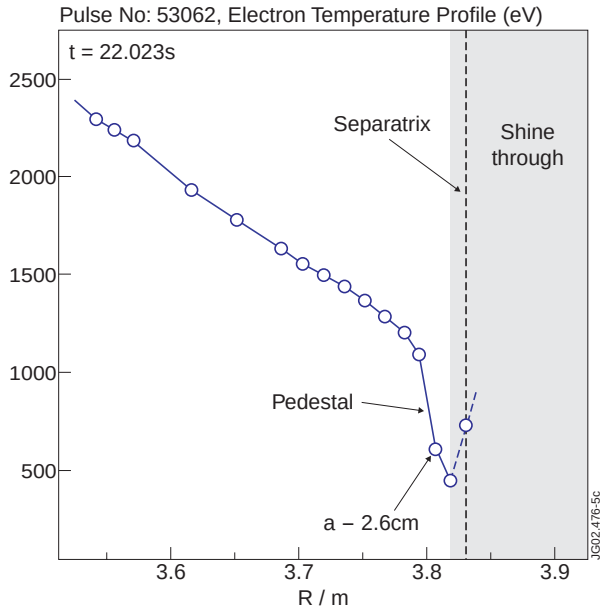

Figure 5: Electron temperature profile as measured by the ECE. The arrow marks the channel where the signal oscillations are most prominent on Fig. 4, supported by the large temperature gradients in the pedestal. The shine-through effect impedes a full coverage of the measurements out to the separatrix.

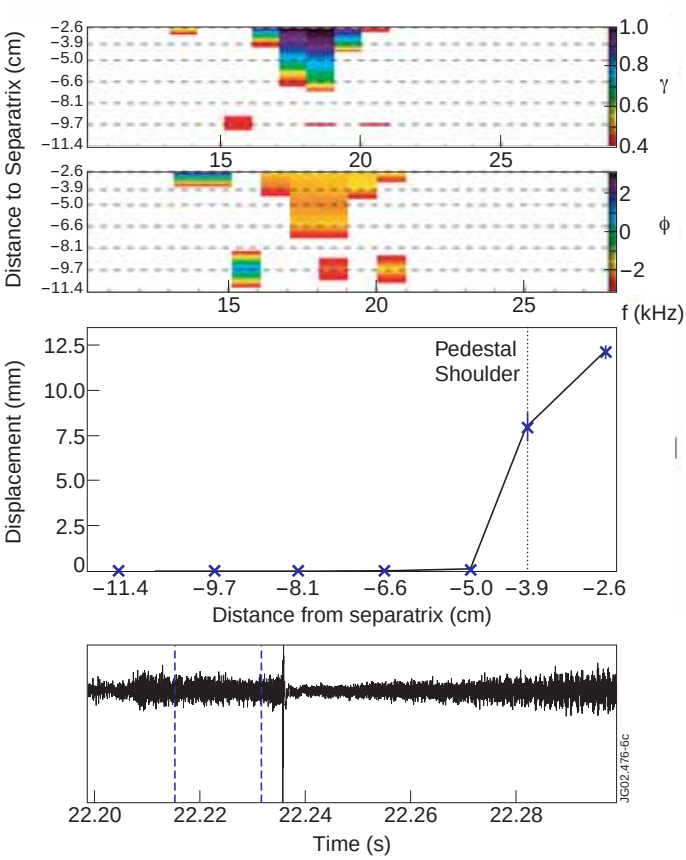

Figure 6: Coherence analysis of a Mirnov coil with the edge ECE channels. The first two plots give the values of the coherence and of the phase of the cross-spectral density, respectively, as a function of frequency and distance to the separatrix. The phase shows no variations with radius, suggesting a kink-like mode. The third window shows the magnitude of the radial mode displacement as a function of radius, and the fourth one shows the the Mirnov signal with the time interval used

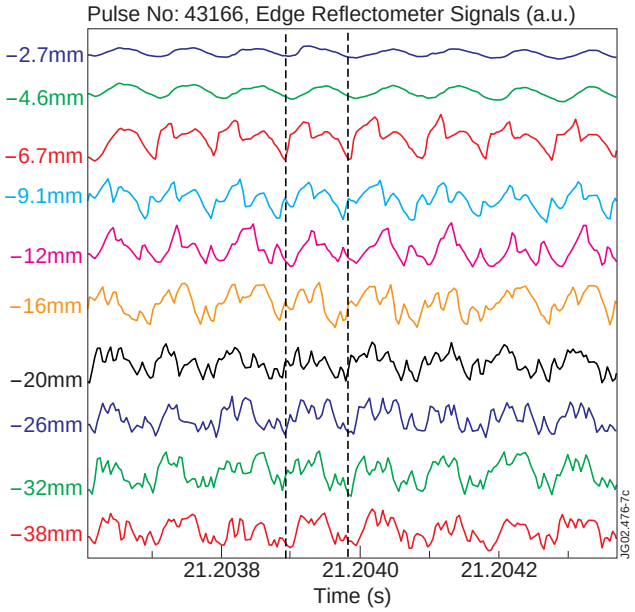

Figure 7: Traces of the 10 edge reflectometer channels together with the radii of the reflecting layers relative to the separatrix radius showing the oscillations corresponding to an n = 8-precursor. The cut-off densities range from 0.43 × 10^{19} m^{-3} (uppermost channel) to 6.0 × 10^{19} m^{-3} (lowermost channel). The dashed lines are to guide the eye.

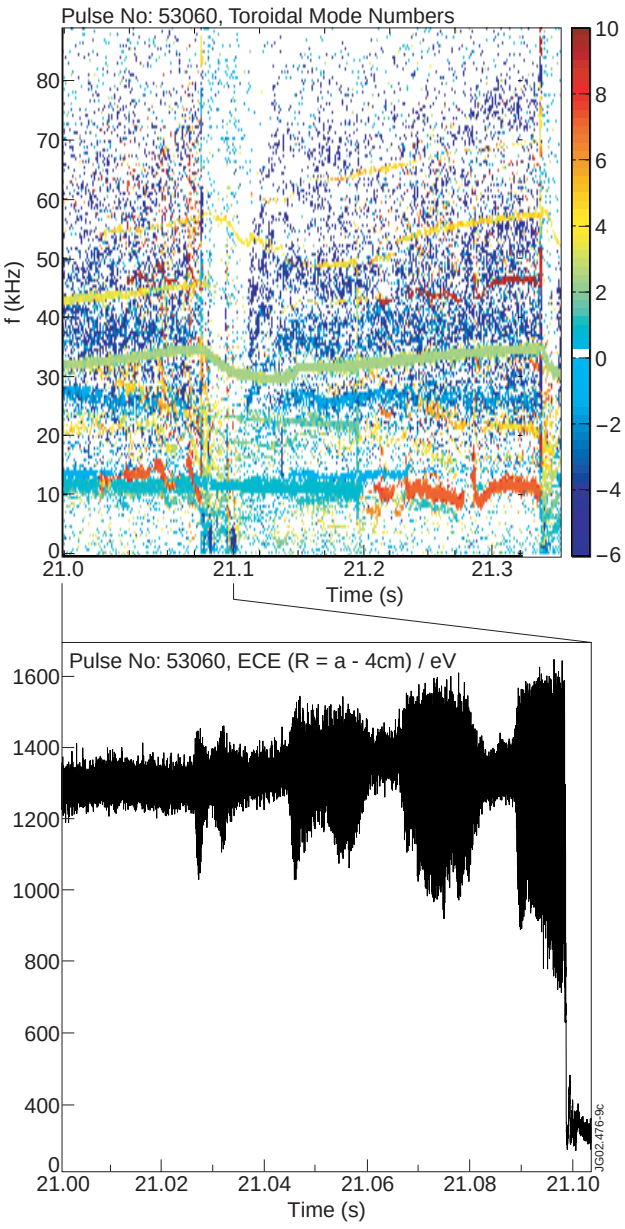

Figure 9: Toroidal mode numbers and ECE emission 4 cms inside the separatrix showing intermittent n =7 precursor modes at 10-15kHz prior to two type-I ELMs at roughly 21.1s and 21.34s, respectively.

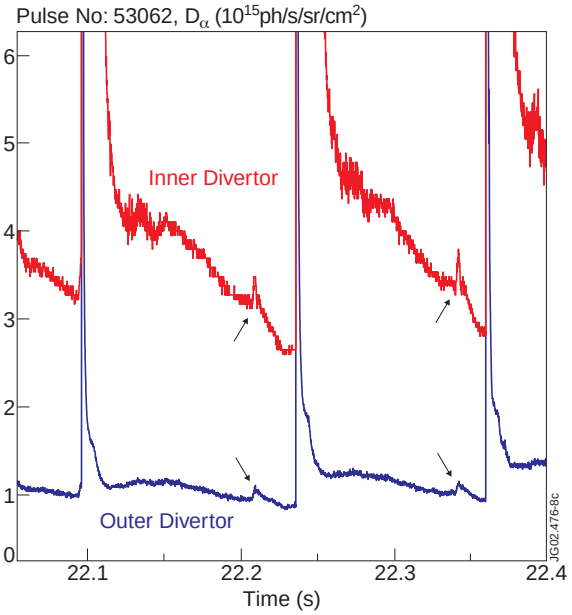

Figure 8. Inner and outer divertor D_α-signals for the example of Fig.2. The arrows point at the time of the precursor onset.

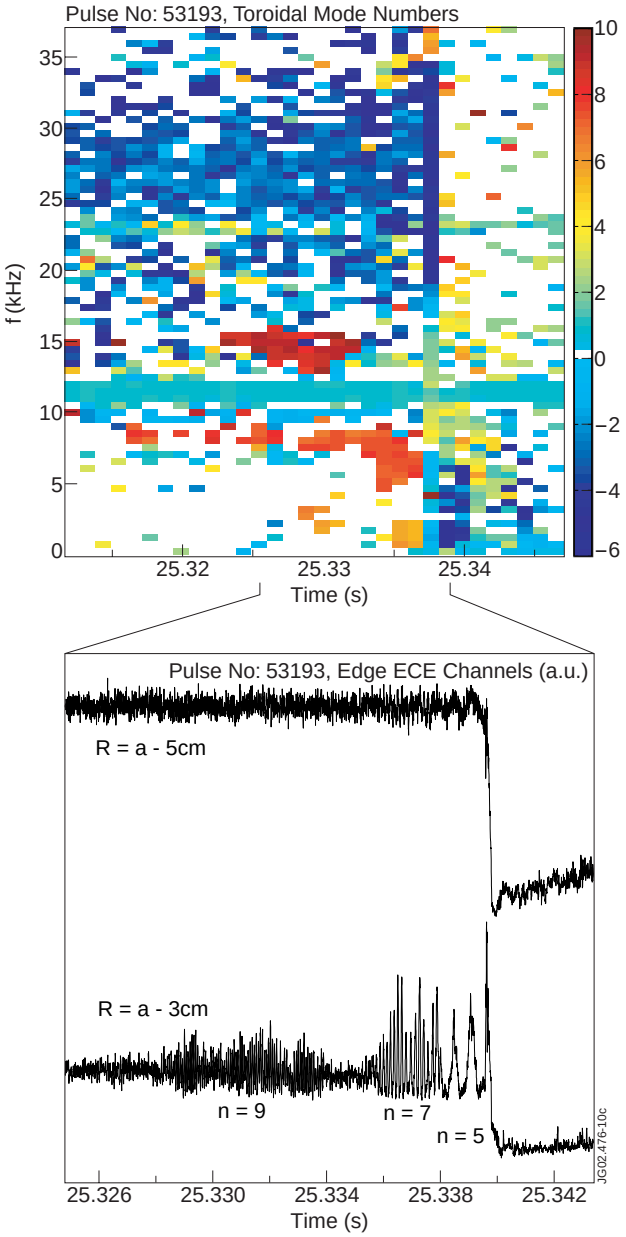

Figure 10: Toroidal mode numbers and ECE emission 5 and 3 cms inside the separatrix, respectively, showing a rapid change of dominant precursors. The continuous mode at 12kHz is a sawtooth precursor.

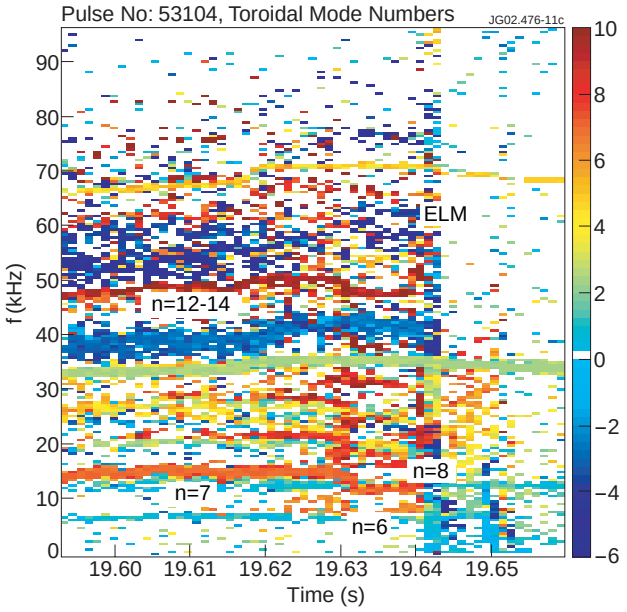

Figure 11. Toroidal mode numbers for an example showing multiple precursors. Also visible is a continuous 4/3 mode around 34 kHz triggered at an earlier time.

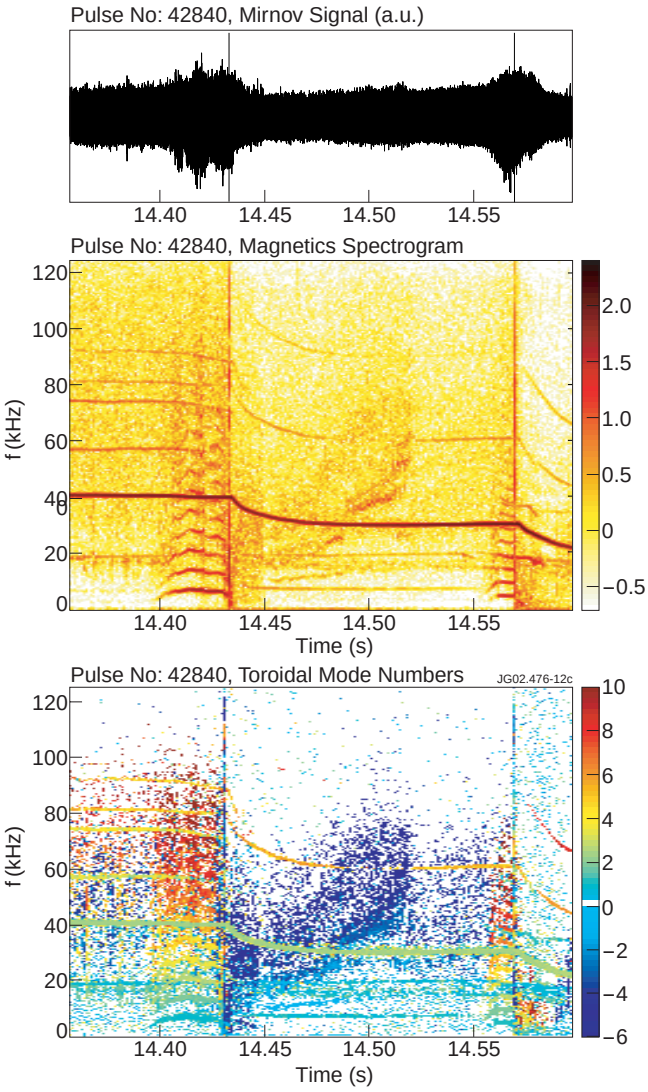

Figure 12. Mirnov signal of a low field side coil, the corresponding spectrogram, and the spectrum of toroidal mode numbers showing two external kinks. The continuous mode with initially 40 kHz is a 4/3-mode. Like the higher-precursors, external kinks propagate in the direction of the ion diamagnetic drift.

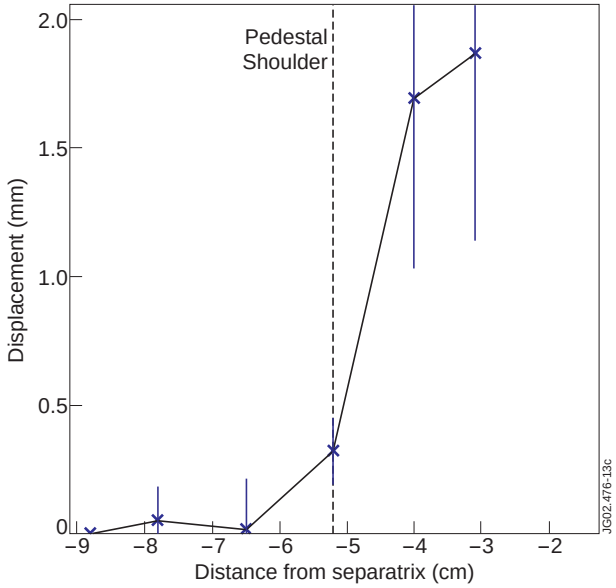

Figure 13. Radial displacement profile of an n = 1 precursor together with position of the pedestal shoulder. Relative to the width of the transport barrier, lower modes are narrower than higher modes.

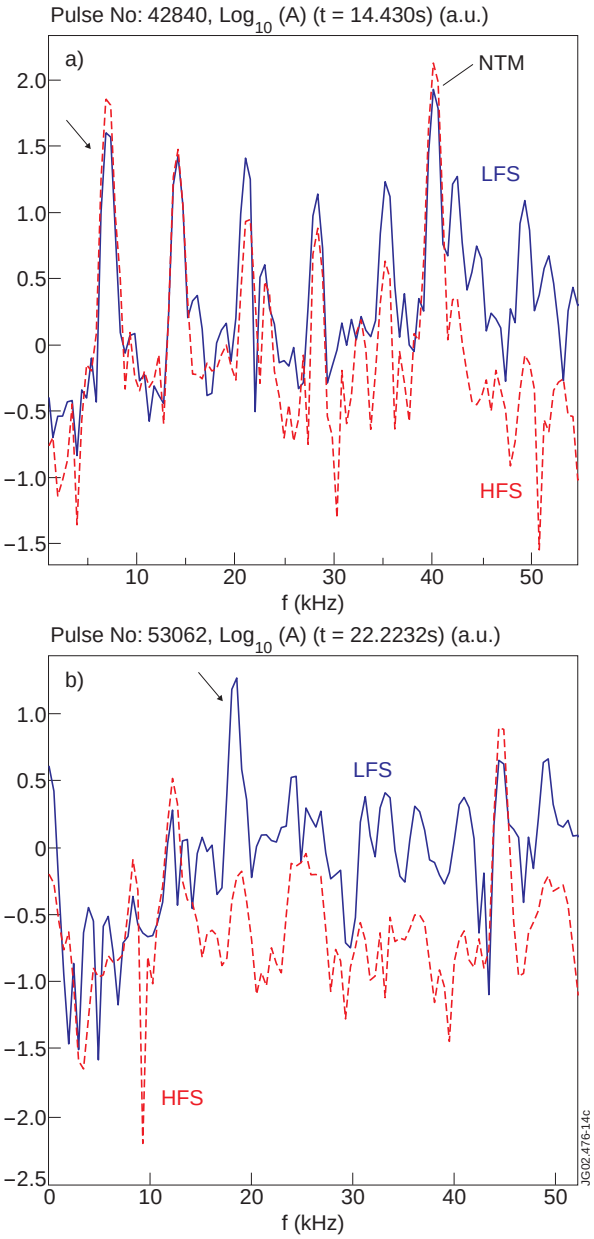

Figure 14. Logarithmic Fourier spectra of Mirnov signals of low/high field side coils with comparable distance to the separatrix a.) for one of the n = 1 precursors of Fig. 12, and b.) for one of the n = 8 precursors of Fig. 2. The arrow points at the precursor contribution. For the n = 1 component at 7kHz the ratio of Fourier amplitudes on the high/low field side is ~1.75, while for the n = 1 precursor n = 8 it is roughly 30.

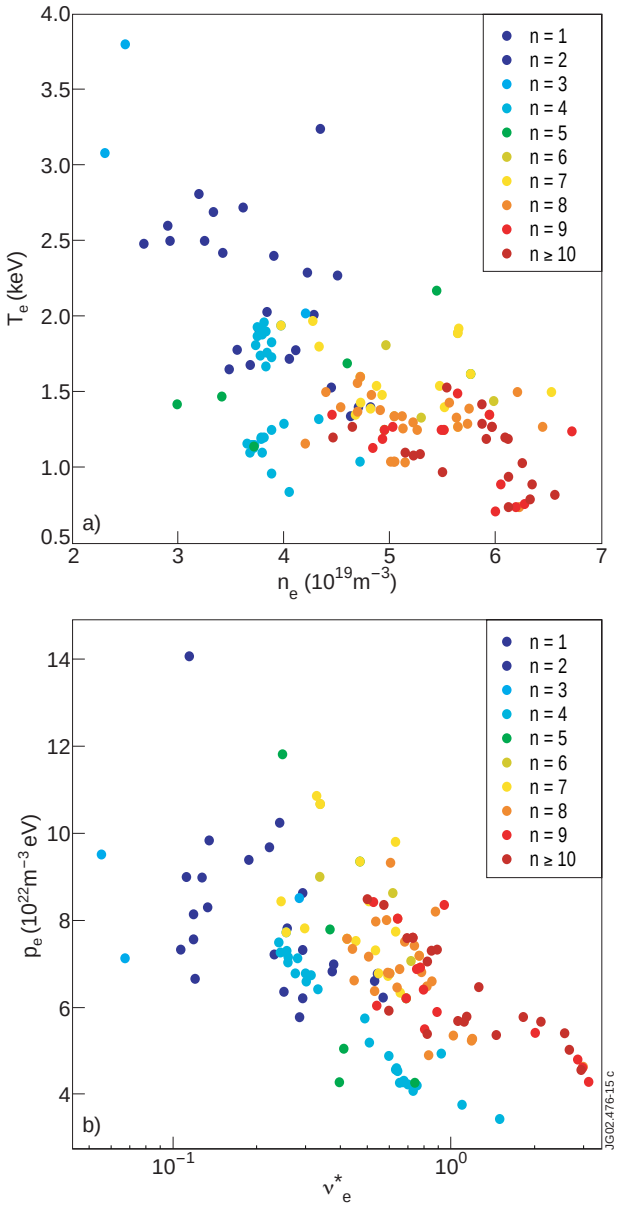

Figure 15: Precursor n-numbers as a function of a.) edge electron temperature and line-averaged density, and b.) electron pedestal pressure and collisionality.

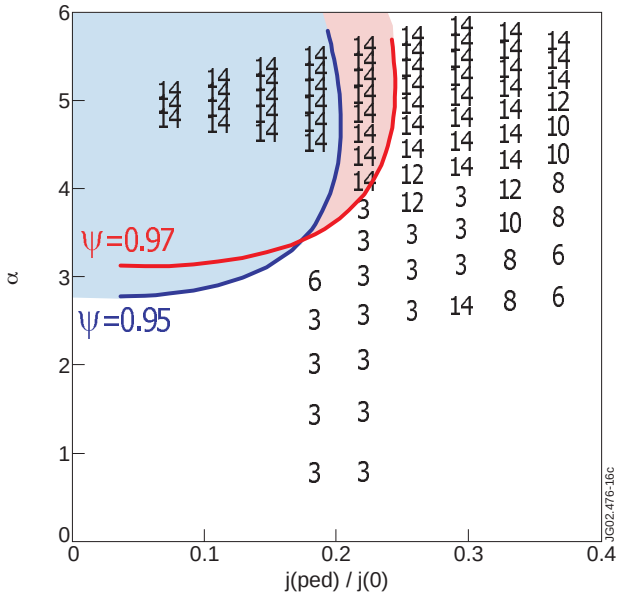

Figure 16: Stability limits for n = 1–14 modes (numbers) and for n=∞ ballooning modes (colored areas) for an ELMy-H discharge.

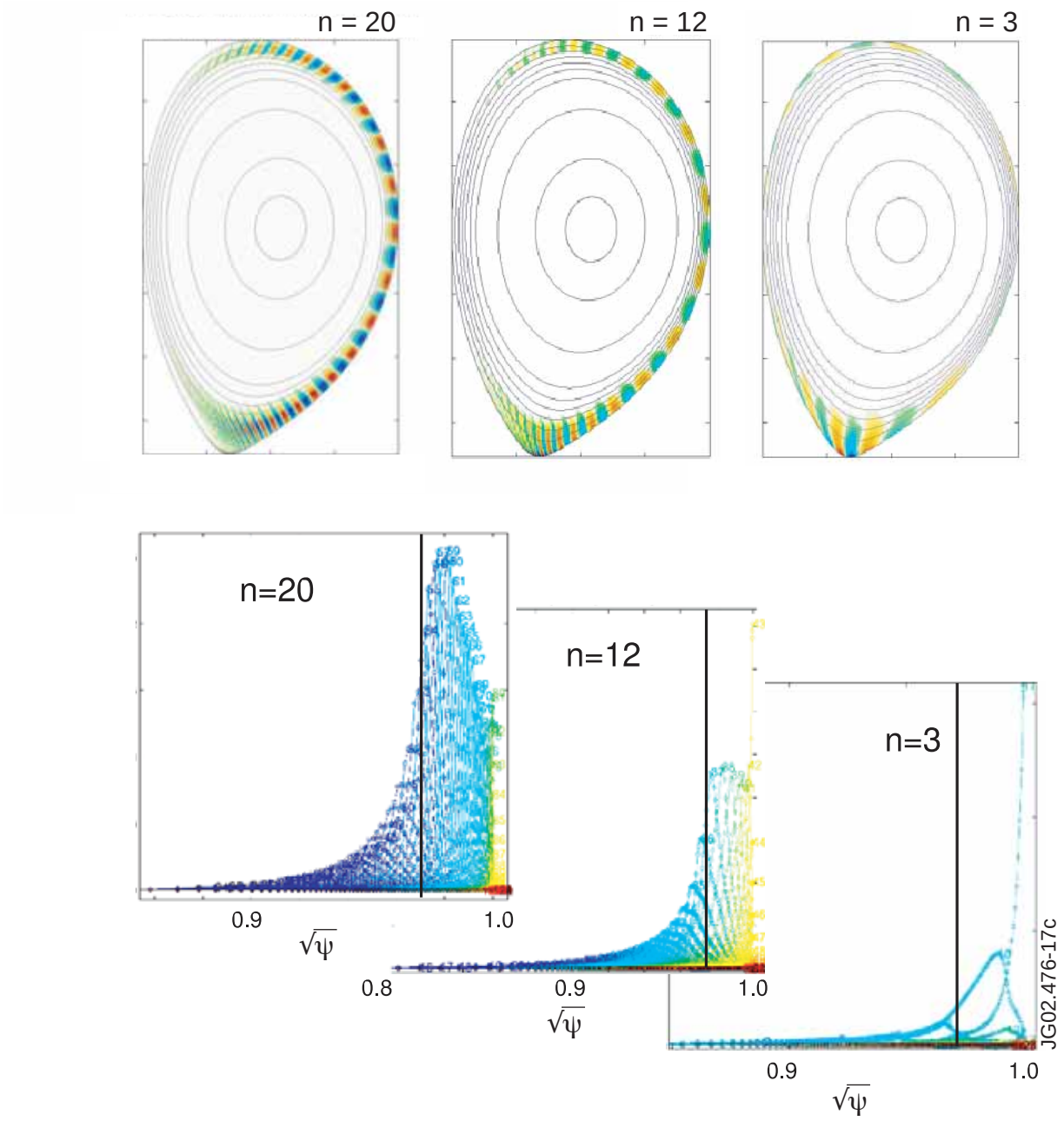

Figure 17. Poloidal structure of the radial displacements of an n = 20 ballooning, an n = 12 ballooning-kink and an n = kink instability together with their midplane radial displacement profiles. Each curve corresponds to a poloidal component with its respective poloidal mode number. The vertical lines denote the position of the pedestal shoulder.